CHEMISTRY OF MATERIALS
Article

Chem. Mater. **2010,** *22,* 2061–2068 2061
DOI:10.1021/cm903315u

Mechanistic Interpretation of the Aurivillius to Perovskite Topochemical Microcrystal Conversion Process

Stephen F. Poterala,*[,†] Yunfei Chang,[†,‡] Trevor Clark,[§] Richard J. Meyer, Jr,[⊥] and Gary L. Messing[†]

[†]*Department of Materials Science & Engineering,* [§]*Materials Research Institute, and* [⊥]*Applied Research Laboratory, Pennsylvania State University, University Park, Pennsylvania, and* [‡]*School of Chemistry and Materials Science, Shaanxi Normal University, Xian, P.R. China*

Received October 29, 2009. Revised Manuscript Received January 4, 2010

The kinetics of topochemical and morphological conversion of platelet-shaped $Na_{3.5}Bi_{2.5}Nb_5O_{18}$, $PbBi_4Ti_4O_{15}$, and $BaBi_4Ti_4O_{15}$ Aurivillius phases to $NaNbO_3$, $PbTiO_3$, and $BaTiO_3$ perovskites were studied. Reaction of the ⟨001⟩ oriented Aurivillius phases with excess Na_2CO_3, $Pb_3(CO_3)_2(OH)_2$, and $BaCO_3$, respectively, yielded high-aspect-ratio perovskite microcrystals with ⟨001⟩ orientation. Only the $Na_{3.5}Bi_{2.5}Nb_5O_{18}$ to $NaNbO_3$ conversion occurred directly, whereas TEM analysis of reacted $BaBi_4Ti_4O_{15}$ and $PbBi_4Ti_4O_{15}$ revealed previously unknown Aurivillius-type intermediate phases with $Bi_2O_2^{2+}$ layers ~86 and ~78 Å apart, respectively. Observations from TEM and field emission SEM show that perovskite crystallites grow from multiple nucleation sites, but become slightly misaligned during growth. This misalignment is caused by a loss of epitaxy with the parent Aurivillius phase and subsequent exfoliation of the particles, likely caused by the expulsion of byproduct Bi_2O_3 liquid on phase boundaries. This conversion process results in substantial microstructure damage, which is healed with an annealing step between 950 and 1050 °C. The pathway for formation of ⟨001⟩ oriented, polycrystalline or single-crystal perovskite platelets is illustrated in a general model for topochemical conversion of Aurivillius phases.

Introduction

High-aspect-ratio platelet- and whisker-shaped perovskite microcrystals have many potential applications in dielectric and piezoelectric materials. These powders would make ideal high-dielectric constant fillers for polymer systems and because of their morphology can be preferentially aligned to achieve optimum properties. A primary use of these microcrystals is to produce highly textured ceramics by templated grain growth (TGG), where they serve as templates to seed oriented grain growth in a perovskite ceramic matrix.[1]

To directly produce oriented perovskite microcrystals with high aspect ratios, growth must be restricted along one or more crystallographic directions. Strongly anisotropic growth is often caused by anisotropic surface energy or nucleation energy, or can be induced by poisoning growth on certain crystal faces. However, these mechanisms do not yield high-aspect-ratio particles in cubic perovskites because of their high symmetry. To achieve high aspect ratios, perovskite platelets or whiskers must be grown below the Curie temperature, severely restricting available processing routes. In one example, hydrothermal synthesis has been utilized to produce high aspect ratio $PbTiO_3$, but these particles are extensively twinned.[2]

Because of the difficulty in directly synthesizing high-aspect-ratio perovskite powders, most successful approaches rely on topochemical conversion of two-dimensional perovskite structures (compounds containing perovskite layers) such as the Ruddlesen−Popper, Dion−Jacobson, or Aurivillius phases. The first production of a three-dimensional perovskite by topochemical conversion was the dehydration of the hydrated layer structure $H_2La_2Ti_3O_{10}$ to produce a defective $La_{2/3}TiO_3$ perovskite.[3] Because of the charge balance in layered structures of this type, dehydration reactions always yield A-site deficient perovskites. Schaak et al. demonstrated the production of defect-free perovskites via a reduction reaction approach.[4] In this case, Dion−Jacobson compounds with the general formula $AEu_2Ti_3O_{10}$ were converted into $AEu_2Ti_3O_9$ perovskites by reduction of Eu^{3+} to Eu^{2+}. Although capable of producing defect-free perovskites, this method is limited to compositions containing easily reducible multivalent cations such as Eu^{3+}.

Although this initial work focused on the production of metastable perovskite phases, similar methods have been utilized to produce conventional perovskite chemistries

*Corresponding author. E-mail: sfp908@psu.edu.

(1) Messing, G. L.; Trolier-McKinstry, S.; Sabolsky, E. M.; Duran, C.; Kwon, S.; Brahmaroutu, B.; Park, P.; Yilmaz, H.; Rehrig, P. W.; Eitel, K. B.; Suvaci, E.; Seabaugh, M.; Oh, K. S. *Crit. Rev. Solid State Mater. Sci.* **2004**, *29*(2), 45.
(2) Suvaci, E.; Anderson, J.; Messing, G. L.; Adair, J. H. *Key Eng. Mater.* **2001**, *206−213*, 163.
(3) Gopalakrishnan, J.; Bhat, V. *Inorg. Chem.* **1987**, *26*, 4299.
(4) Schaak, R. E.; Mallouk, T. E. *J. Am. Chem. Soc.* **2000**, *122*, 2798.

Published on Web 02/04/2010

with highly controlled morphology. The first use of topochemical conversion for this purpose was the production of ⟨001⟩ oriented tabular $SrTiO_3$ by Watari et al. in 2000.[5] In this work, the Ruddlesen−Popper phase $Sr_3Ti_2O_7$ was reacted with excess TiO_2 in a KCl flux at temperatures between 1000 and 1200 °C. During conversion, the $SrTiO_3$ phase was shown to nucleate on the (001) $Sr_3Ti_2O_7$ surfaces and grow inward, eventually consuming the precursor phase. Since this work, the use of precursor phases as structural templates to produce high-aspect-ratio perovskite microcrystals has been termed topochemical microcrystal conversion (TMC) because the precursor phase controls both the orientation and the morphology of the resulting perovskite phase. Subsequently, Saito et al. developed a method to form higher aspect ratio ⟨001⟩ $SrTiO_3$ by converting $SrBi_4Ti_4O_{15}$ in a KCl flux.[6] The authors attribute the higher aspect ratio to a reduced conversion temperature (950 °C).

The TMC method has been developed to the greatest extent in the $BaTiO_3$ system. ⟨001⟩ $BaTiO_3$ platelets 5−10 μm in size and 0.5 μm thick were produced by Zhou et al. by conversion of $BaBi_4Ti_4O_{15}$ in a (Na,K)Cl flux.[7] ⟨110⟩ $BaTiO_3$ has been produced by two separate methods. Feng et al. produced ⟨110⟩ oriented platelet $BaTiO_3$ in a two-step hydrothermal conversion of the lepidocrocite-like $K_{0.8}Ti_{1.73}Li_{0.27}O_4$ phase.[8] In a method developed by Sato et al., ⟨110⟩ $BaTiO_3$ is formed in situ by topochemical conversion of acicular ⟨001⟩ TiO_2 (rutile).[9] Sato et al. also produced ⟨111⟩ $BaTiO_3$ microcrystals by the reaction of $Ba_6Ti_{17}O_{40}$ with excess $BaCO_3$.[10] Tabular particles with an aspect ratio around 5 were obtained by this method. Topochemical conversion has also been used to produce ⟨001⟩ oriented platelets of $CaTiO_3$, $NaNbO_3$, $KNbO_3$, and $Na_{0.5}Bi_{0.5}TiO_3$.

The majority of TMC processes use Aurivillius phase precursor compounds, represented by the structural formula $[Bi_2O_2]A_{n-1}B_nO_{3n+1}$, because these phases typically undergo strongly anisotropic growth and thus show high aspect ratios. Despite numerous reports on topochemical conversion, the mechanism of the Aurivillius to perovskite conversion has not been reported in detail. In the reaction of $Sr_3Ti_2O_7$ to $SrTiO_3$, the perovskite phase was observed by TEM to nucleate and grow from the (001) surfaces of the precursor phase.[5] However, the Aurivillius to perovskite reaction is necessarily more complicated by the need to remove Bi_2O_3 from the precursor phase. In this work, the Aurivillius to perovskite TMC reaction was studied by differential thermal analysis (DTA), X-ray diffraction, field-emission SEM, and TEM. The mechanisms of the TMC reaction are reported and used to develop a general model for this process. The three systems selected for study ($PbTiO_3$, $BaTiO_3$, and $NaNbO_3$) are of practical importance, as they are well-suited for TGG in $Pb(Mg_{1/3}Nb_{2/3})O_3$−$PbTiO_3$-, $BaTiO_3$-, and (K,Na)NbO_3-based piezoelectric materials, respectively.

Experimental Procedures

Synthesis of Aurivillius Precursor Phases. *$BaBi_4Ti_4O_{15}$*. Barium bismuth titanate was produced by the method outlined by Liu et al, using bismuth titanate ($Bi_4Ti_3O_{12}$) as a precursor.[7] Bismuth titanate was synthesized by reacting stoichiometric amounts of Bi_2O_3 (Alfa Aesar) and TiO_2 (Evonik Degussa P25) in an equal weight of KCl−NaCl flux (50:50 molar ratio). The mixture was ball-milled in ethanol for 12 h, dried, and reacted at 1100 °C for 1−2 h in a covered Al_2O_3 crucible. The flux was removed by washing with deionized water at 75 °C. $Bi_4Ti_3O_{12}$ was then reacted with $BaCO_3$ (Baker Analytical) and TiO_2 in a 1:1.1:1.1 molar ratio in a $BaCl_2$−KCl flux (1:1 molar ratio). The $BaCO_3$, TiO_2, $BaCl_2 \cdot 2H_2O$, and KCl powders were ball-milled in ethanol for 12 h, and reacted at 1080 °C for 1 h in a covered Al_2O_3 crucible. The flux was removed by washing with deionized water at 75 °C.

$PbBi_4Ti_4O_{15}$. Lead bismuth titanate was synthesized using $Pb_3(CO_3)_2(OH)_2$ (Sigma-Aldrich), Bi_2O_3, and TiO_2 powders in an equal weight of KCl flux. The mixed powders were ball-milled in ethanol for 12 h and reacted at 1050 °C for 1−2 h in a covered Al_2O_3 crucible. The flux was removed by washing in deionized water at 75 °C.

$Na_{3.5}Bi_{2.5}Nb_5O_{18}$. Sodium bismuth niobate was synthesized by the method outlined by Chang et al.[11] Stoichiometric amounts of Na_2CO_3, Bi_2O_3, and Nb_2O_5 powders were mixed with NaCl salt in a 1:1.5 weight ratio. The powders were ball-milled in ethanol for 12 h, and then reacted at 1125 °C for 2−6 h in a covered Al_2O_3 crucible. The flux was removed by washing with deionized water at 75 °C.

Topochemical Microcrystal Conversion. To study the Aurivillius to perovskite conversion, samples of each precursor phase were mixed with $Pb_3(CO_3)_2(OH)_2$ (50% excess), $BaCO_3$ (33% excess), or Na_2CO_3 (100% excess) powders and salt fluxes in a 1:1 weight ratio (KCl, $Na_{0.5}K_{0.5}Cl$, and NaCl for synthesis of $PbTiO_3$, $BaTiO_3$, and $NaNbO_3$, respectively). The salts and carbonate powders were mixed by ball milling in high purity ethanol for 12 h, after which the Aurivillius platelet particles were added by magnetic stirring at 200 rpm. After evaporating the ethanol, 2−3 g samples of each precursor mixture were heated at 8 °C/min to temperatures between 500 and 1150 °C and air quenched. Samples heated to less than 1000 °C were reacted in Al_2O_3 crucibles, and samples heated to 1000 °C or higher were reacted in platinum crucibles. After the synthesis study, larger batches (5−10 g) of templates were synthesized at optimized conversion temperatures for each system (950 °C for $BaTiO_3/Na_{0.5}K_{0.5}Cl$, 975 °C for $NaNbO_3$/NaCl, and 1050 °C for $PbTiO_3$/KCl) to observe the final microstructure of the perovskite microcrystals. The salt flux was removed by washing with DI water at 75 °C, after which byproduct Bi_2O_3 was removed by soaking in 30% HNO_3 for 1−3 h. The microcrystals were then dispersed by ultrasonicating and rinsed 5 times with deionized water.

Characterization Techniques. Small samples (∼1 g) of reacted powders, prepared as described above, were ground in a mortar and pestle and studied via X-ray diffraction (PANalytical with PIXcel detector, Cu K_α radiation). Front loading sample

(5) Watari, K.; Brahmaroutu, B.; Messing, G. L.; Trolier-McKinstry, S.; Cheng, S. *J. Mater. Res.* **2000**, *15*, 846.
(6) Saito, Y.; Takao, H. *Jpn. J. Appl. Phys.* **2006**, *45*, 7377.
(7) Liu, D.; Yan, Y.; Zhou, H. *J. Am. Chem. Soc.* **2007**, *90*, 1323.
(8) Feng, Q.; Hirasawa, M.; Yanagisawa, K. *Chem. Mater.* **2001**, *13*, 290.
(9) Sato, T.; Yoshida, Y.; Kimura, T. *J. Am. Ceram. Soc.* **2007**, *90*(9), 3005.
(10) Sato, T.; Kimura, T. *Ceram. Int.* **2008**, *34*, 757.
(11) Chang, Y.; Yang, Z.; Chao, X.; Liu, Z.; Wang, Z. *Mater. Chem. Phys.* **2008**, *111*, 195.

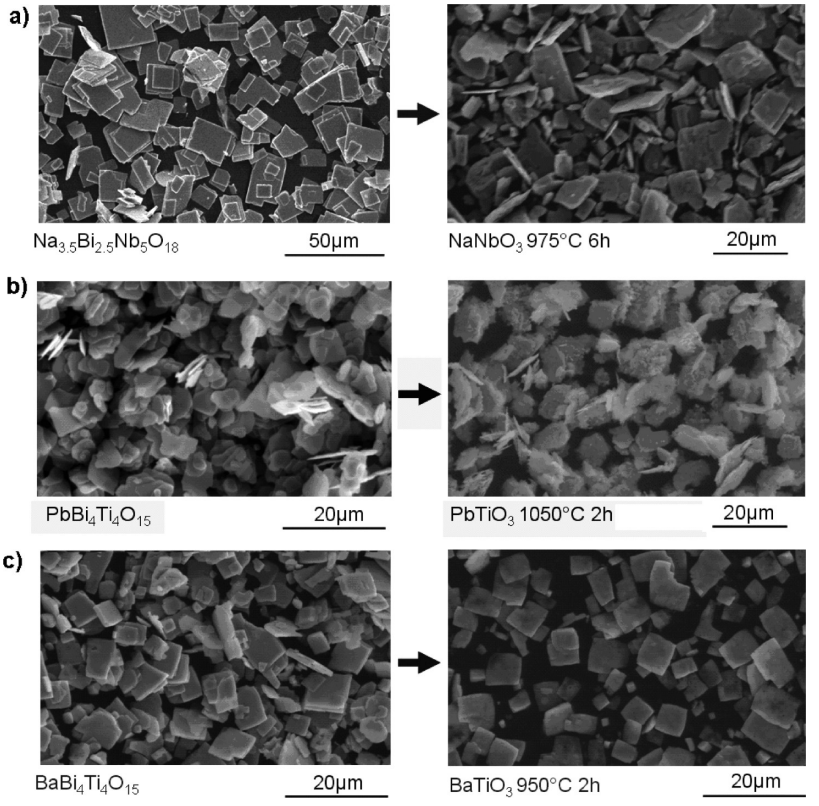

Figure 1. SEM image comparison of Aurivillius and perovskite microcrystals for the (a) $NaNbO_3$, (b) $PbTiO_3$, and (c) $BaTiO_3$ systems. The reaction temperature for each process is noted.

holders (zero background silicon) were used with fixed area geometry (step size = 0.01°, count time = 5 s, sample area = 25 mm^2). Phases in each sample were identified using the software package MDI Jade 9. To study phase evolution, we measured the total peak area for each phase of interest by profile fitting only the relevant peaks in each data set, after subtracting background. To complement the XRD results, we analyzed 50−100 mg samples of precursor mixtures, prepared as described above, by thermogravimetric analysis (TGA, TA TGA 2050) and differential thermal analysis (DTA, TA DSC 2920). During TGA, samples were heated in an open Pt pan at 8 °C/min from room temperature to 1000 °C to determine the temperatures at which carbonate decomposition and salt evaporation occurred. DTA was performed in closed Pt pans to minimize salt evaporation, and data was collected from room temperature to 1400 °C.

Morphologic evolution of the template particles during TMC was studied by FESEM (JEOL 6700F). Samples for FESEM analysis were heated to 675−800 at 8 °C/min and immediately air quenched. These samples were selected based on XRD data for each system to contain both Aurivillius and perovskite phases (700 °C for $BaTiO_3$, 750 °C for $PbTiO_3$, and 700 °C for $NaNbO_3$, as described in the previous subsection). No powder preparation (grinding, washing, etc.) was used so as to avoid damaging fine morphology features on the platelike particle surfaces. Samples of each powder were dispersed on carbon tape and coated with Ir to prevent charging. SEM was conducted at an accelerating voltage of 2 kV and working distance of 3 mm. To observe morphology and phase structure at a finer scale, we thinned the platelets in cross-section via focused ion beam (FIB, FEI Quanta 200 3D) and observed via TEM (Philips EM420T). Preparation for such thinning involves dispersing the dry powders on single-crystal Si substrates, selecting platelets that are lying flat, and transferring the platelets to TEM grids via a manipulator. Cross-sections were cut perpendicular to the platelet normal, close to an expected ⟨001⟩ perovskite zone axis. Thinning was performed at 30 kV with final cleaning at 5 kV before bright-field TEM observation.

Results and Discussion

Characterization of Aurivillius and Perovskite Phases. SEM images of Aurvillius precursor and perovskite product powders for each reaction are shown in Figure 1. The $BaBi_4Ti_4O_{15}$ and $PbBi_4Ti_4O_{15}$ phases were synthesized at temperatures between 1050 and 1100 °C, respectively, and were both 5−15 μm in size. Despite a similar synthesis temperature, $Na_{3.5}Bi_{2.5}Nb_5O_{18}$ grew faster and reached larger sizes of 25−50 μm. All precursor phases could be easily synthesized with aspect ratios greater than 10:1. Although $BaBi_4Ti_4O_{15}$ and $Na_{3.5}Bi_{2.5}Nb_5O_{18}$ formed square platelets, $PbBi_4Ti_4O_{15}$ grew with a more irregular morphology.

The phase composition of each precursor powder is shown in Figure 2. All Aurivillius powders showed good crystallinity. No impurity phases were detected in the $PbBi_4Ti_4O_{15}$ sample, whereas the $Na_{3.5}Bi_{2.5}Nb_5O_{18}$ and $BaBi_4Ti_4O_{15}$ samples contained small amounts of unidentified phases, denoted in Figure 2.

The XRD patterns for each perovskite phase are shown in Figure 3. The $BaTiO_3$ and $NaNbO_3$ powders were phase pure or nearly phase pure, whereas the $PbTiO_3$ powder contained a substantial impurity phase denoted by the extra peak near 31° 2θ. This 2θ value is near the 100% intensity peak for many Aurivillius phases in the

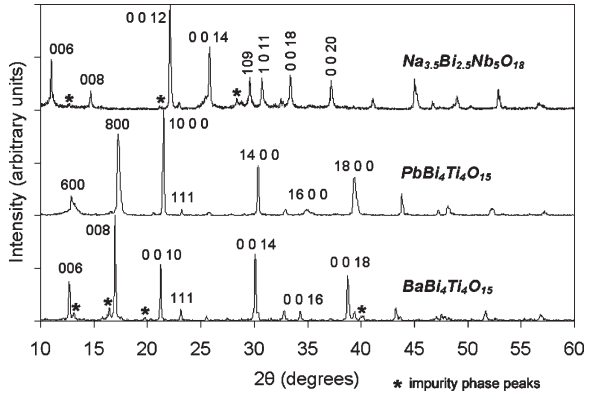

Figure 2. XRD patterns of Aurivillius TMC precursor phases. Major peaks are indexed using ICDD PDF 00−042−0399 ($Na_{3.5}Bi_{2.5}Nb_5O_{18}$), PDF 04−008−9705 ($PbBi_4Ti_4O_{15}$), and PDF 01−073−2859 ($BaBi_4Ti_4O_{15}$). Second phase peaks in each sample are also indicated.

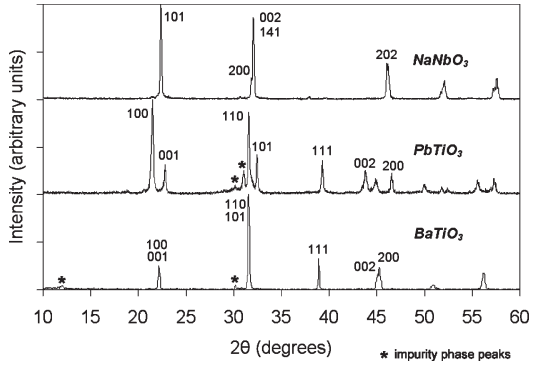

Figure 3. XRD patterns of perovskite microcrystals synthesized via TMC. Peaks are indexed using ICDD PDF 00−033−1270 ($NaNbO_3$), PDF 01−073−7551 ($PbTiO_3$), and PDF 04−008−2416 ($BaTiO_3$). Impurity phases are also indicated.

$PbTiO_3$−$Bi_4Ti_3O_{12}$ binary system. During each TMC reaction, the morphology of the derived perovskite phase was the same as the precursor Aurivillius phase.

Phase Formation during the TMC Process. The phase evolution of reacted Aurivillius phases with respect to temperature is shown in Figure 4. As shown in Figure 4c, only $NaNbO_3$ formed directly from the precursor phase. Thus, it is inferred that no stable intermediate compounds exist between $Na_{3.5}Bi_{2.5}Nb_5O_{18}$ and $NaNbO_3$. In contrast, intermediate bismuth layer structures (possibly Aurivillius phases with $n > 4$) related to $PbTiO_3$ and $BaTiO_3$ were detected at temperatures >700 °C. These phases could not be indexed definitively by XRD because in all cases only one clear peak was observed around 30.5° 2θ (near the 100% intensity peak for $n > 4$ Aurivillius phases). These peaks were also very broad, suggesting low crystallinity. The intermediate bismuth layer structure phase(s) were found to be most persistent during the synthesis of $PbTiO_3$. This is attributed to the large number of stable intermediate Aurivillius phases in this system (compounds with $n = 5$, 6, and 7 are known).[12,13] Although intermediate phases persisted even to the highest temperature studied (1150 °C), they were partially eliminated with longer soaking times.

(12) Tellier, J.; Boullay, P.; Mercurio, D *Z. Kristallogr.* **2007**, *222*(5), 234.
(13) Kikuchi, T. *Mater. Res. Bull.* **1979**, *14*, 1561.

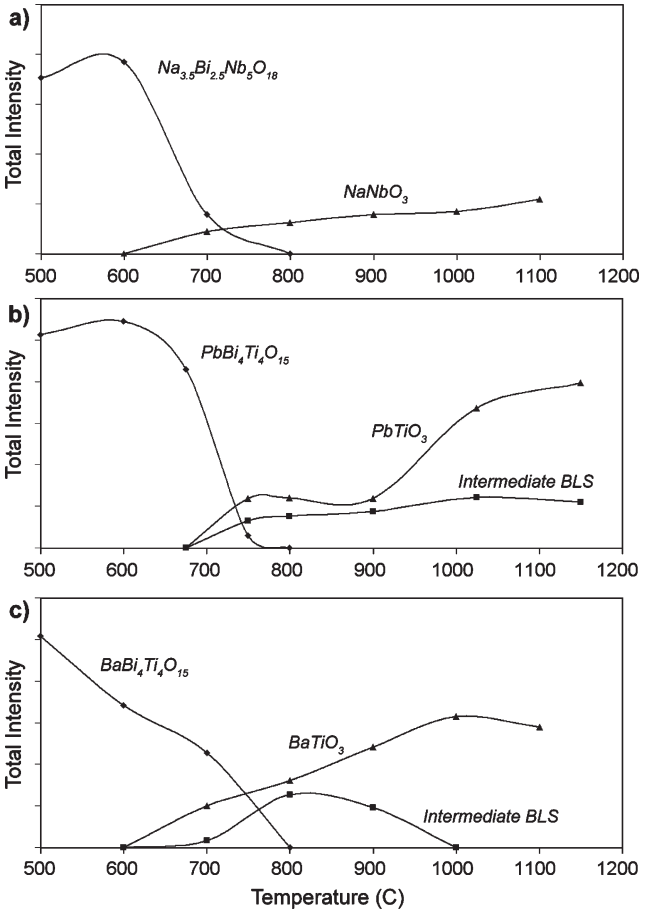

Figure 4. Phase evolution in (a) $BaTiO_3$, (b) $PbTiO_3$, and (c) $NaNbO_3$ systems as measured by total XRD peak intensity, showing relative amounts of Aurivillius, perovskite, and intermediate bismuth layer structure (BLS) phases.

Energy-dispersive spectroscopy (EDS) was used to determine the approximate amount of bismuth remaining in each system after topochemical conversion. In the case of $NaNbO_3$, no bismuth was detected after 6 h, whereas $BaTiO_3$ and $PbTiO_3$ templates produced after 2 h both contain measurable bismuth. The bismuth content in $BaTiO_3$ microcrystals was estimated to be $< 5\%$ on an A-site basis, whereas the content in $PbTiO_3$ microcrystals is as high as 25%. This bismuth is likely accommodated by the impurity phase(s) observed during X-ray diffraction.

Differential thermal analysis (DTA) and thermogravimetric analysis (TGA) were used to complement the XRD study on phase formation (Figure 5). The TGA data, Figure 5a, show the endothermic decomposition temperatures of Na_2CO_3, $BaCO_3$, and $Pb_3(CO_3)_2(OH)_2$. This weight loss occurs at 625 °C for $BaCO_3$, 300−400 °C for $Pb_3(CO_3)_2(OH)_2$, and 650 °C for Na_2CO_3, respectively. These decomposition reactions also appear in the DTA data Figure 5b. In addition, strong endothermic peaks are observed because of the melting of the salt fluxes (770 °C for KCl in the $PbTiO_3$ system, 801 °C for NaCl in the $NaNbO_3$ system, and ~650 °C for (K,Na)Cl in the $BaTiO_3$ system). Samples of pure Na_2CO_3 and $BaCO_3$ were also analyzed for comparison to these data and did not show significant weight loss below 800 °C. This indicates that the decomposition of Na_2CO_3 and

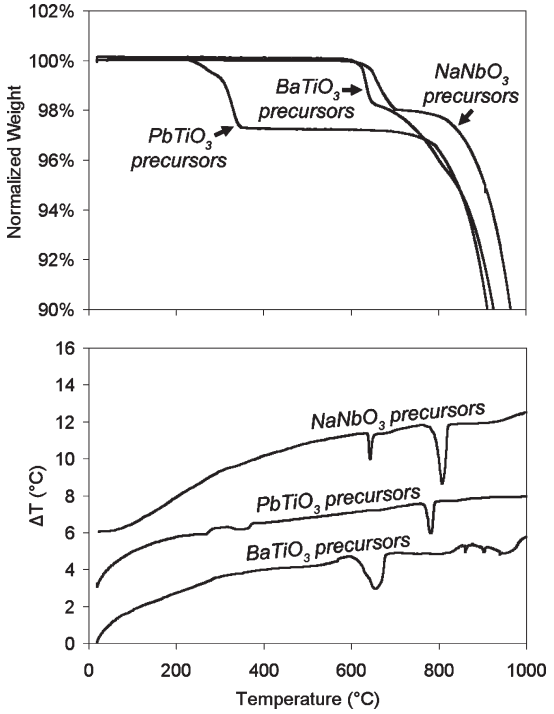

Figure 5. Thermal characterization of the Aurivillius to perovskite conversion via (a) TGA and (b) DTA. Powder mixtures for synthesizing each perovskite phase (prepared as described in Experimental Procedures) were heated at 8 °C/min in platinum pans.

$BaCO_3$ is caused by the direct reaction of these carbonates with the Aurvillius precursors.

Reaction temperatures of 625−650 °C correspond well to those observed by XRD. Unfortunately, the strong endotherm associated with CO_2 removal masks any possible signal intrinsic to the Aurivillius to perovskite conversion. In contrast, $Pb_3(CO_3)_2(OH)_2$ decomposes between 300 and 400 °C, below the temperature where any reaction of the Aurivillius phase $PbBi_4Ti_4O_{15}$ is observed to occur via XRD. Although the appearance of new phases is confirmed via XRD at ≤750 °C, the DTA data for this system show no visible peaks in this range. This implies that the topochemical reaction is not strongly endothermic or exothermic.

Microstructure Development during TMC. Figure 6 shows FESEM images of microcrystals (viewed edge-on) in each system after reaction at temperatures between 700 and 750 °C. In all systems, exfoliation of the platelike microcrystals was observed to occur during the TMC process. Exfoliation was observed to be most extensive in the $PbTiO_3$ system, with most particles showing a visibly layered structure. Individual lamina were 100−200 nm thick and 1−5 μm in diameter.

Exfoliation was also observed in many $BaTiO_3$ and $PbTiO_3$ samples which were reacted at temperatures sufficient to produce the perovskite phase (~950 °C or higher) but were held at this temperature for less than the times specified in the Experimental Procedures. After digesting the byproduct Bi_2O_3 with 30% HNO_3 solution, the resulting samples contained submicrometer- or micrometer-sized, high-aspect-ratio perovskite particles, in addition to larger platelike microcrystals.

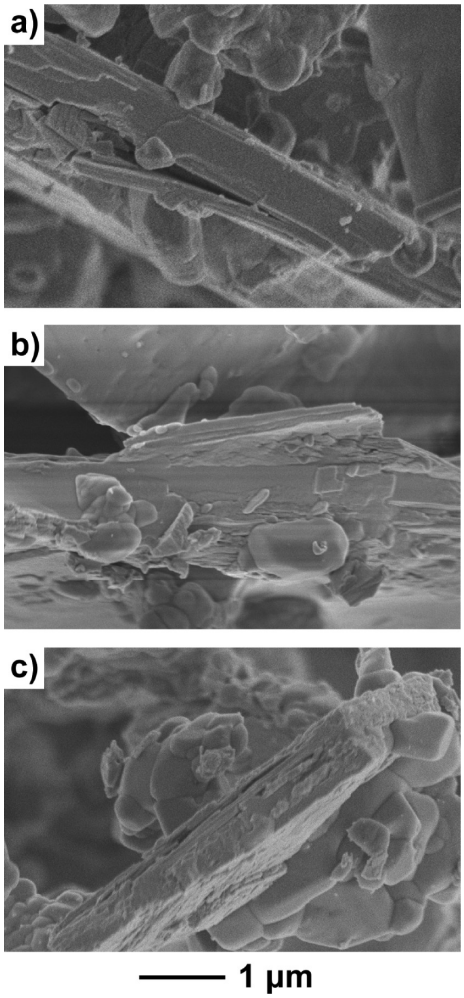

Figure 6. FESEM images showing exfoliation of partially reacted Aurivillius particles during topochemical conversion for (a) $Na_{3.5}Bi_{2.5}Nb_5O_{18}$ (800 °C−1 min), (b) $PbBi_4Ti_4O_{15}$ (750 °C−1 min), and (c) $BaBi_4Ti_4O_{15}$ (800 °C−1 min).

To better observe the path of the TMC reaction, we prepared TEM samples from $BaBi_4Ti_4O_{15}$ and $PbBi_4Ti_4O_{15}$ microcrystals reacted at 700 and 750 °C, respectively. A bright field TEM image of the $BaBi_4Ti_4O_{15}$ sample is shown in Figure 7. After reaction at 700 °C, the observed particle contained a mixture of $BaBi_4Ti_4O_{15}$ and $BaTiO_3$ phases, as well as an intermediate bismuth layer structure (BLS) phase.

After being heated to 700 °C, the observed particle contained an unreacted core of $BaBi_4Ti_4O_{15}$ crystal surrounded by $BaTiO_3$ grains that nucleated near the particle surface. These $BaTiO_3$ grains are not perfectly aligned with each other or the parent $BaBi_4Ti_4O_{15}$ phase, as evidenced by the fact that only one large $BaTiO_3$ grain is strongly diffracting in the TEM image. A large reaction layer containing intermediate phase(s) is also present, along with numerous structural defects and pores. These defects and pores are generally parallel to the microcrystal surfaces, and likely are related to exfoliation observed under FESEM. A closer view of this intermediate region (Figure 8) shows a mixture of intermediate BLS phase and poorly crystalline $BaTiO_3$ grains.

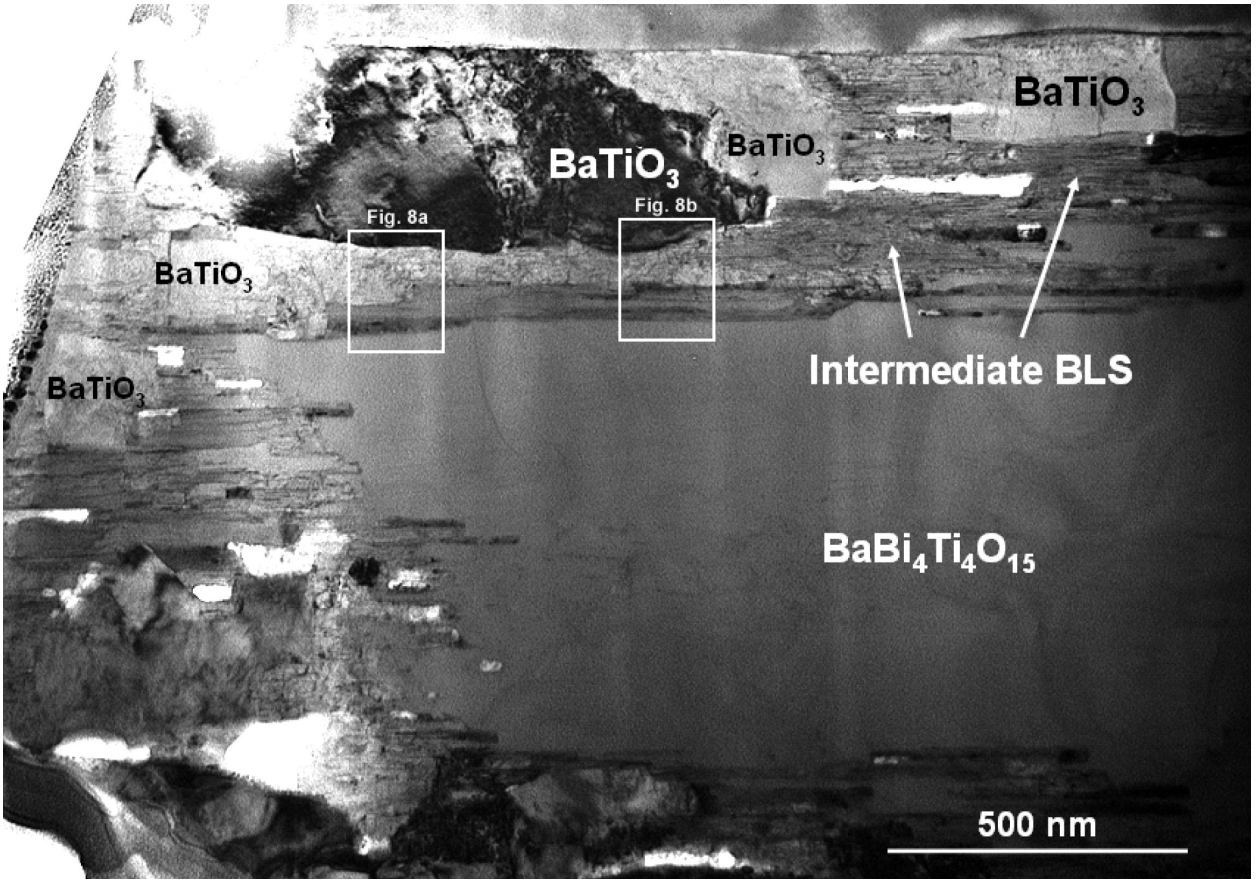

Figure 7. Bright-field TEM image of $BaBi_4Ti_4O_{15}$ after partial conversion into $BaTiO_3$ at 700 °C, showing nucleation of $BaTiO_3$ at multiple sites. Insets show the location of images in Figure 8.

The TEM orientation was rotated a few degrees between adjacent images a and b in Figure 8 to illustrate the misalignment between the large $BaTiO_3$ grains, the poorly crystalline $BaTiO_3$, and the $BaBi_4Ti_4O_{15}$ core, and to show detail in each of these regions. The total misalignment between the large $BaTiO_3$ grain at the top of Figure 8 and the unreacted $BaBi_4Ti_4O_{15}$ core was about 8°. The dotted line in Figure 8a shows the boundary between the intermediate BLS and the $BaTiO_3$ phase regions. The $BaTiO_3$ and $BaBi_4Ti_4O_{15}$ phases were confirmed by electron diffraction (Figure 8c,e). Electron diffraction for the intermediate region, Figure 8d), shows a mixture of $BaTiO_3$ and a poorly crystalline BLS phase, resulting in smeared diffraction spots between those of the $BaTiO_3$. Assuming a pseudotetragonal (*I*4/*mmm*) Aurivillius structure, these diffraction spots represent lattice dimensions of $d_{100} = 3.93$ Å ± 0.03 Å and $d_{002} = 42.90$ Å ± 0.03 Å. The composition of this phase could not be estimated by EDS because of the intermixing of this phase with nanocrystalline $BaTiO_3$.

Figure 9 shows bright-field TEM images of a platelike particle in the $PbTiO_3$ system. The particle imaged consisted primarily of a $PbTiO_3$−$PbBi_4Ti_4O_{15}$ intermediate phase, and contains a small residual core of $PbBi_4Ti_4O_{15}$.

As can be seen in Figure 9a, not all regions of this intermediate phase are diffracting strongly, showing that multiple incoherent grains are present. Figure 9b shows a magnified image of the boundary between $PbBi_4Ti_4O_{15}$ and this intermediate phase. The bismuth oxide layers in this intermediate phase are poorly ordered. Diffraction patterns for the $PbBi_4Ti_4O_{15}$ phase and $PbBi_4Ti_4O_{15}$−$PbTiO_3$ intermediate are shown in panels c and d in Figure 9, respectively. The diffraction spots for the $PbBi_4Ti_4O_{15}$ phase match well with the lattice parameters measured by XRD on unreacted samples of this phase. Assuming a pseudotetragonal (*I*4/*mmm*) Aurivillius structure, the diffraction spots for the intermediate phase represent lattice dimensions of $d_{100} = 3.89$ Å ± 0.03 Å and $d_{002} = 39.27$ Å ± 0.03 Å. EDS analysis of this region indicates a highly Pb-rich composition, suggesting that the observed structure represents a unique Aurivillius-type phase and not a superlattice structure.

Model for the Aurivillius to Perovskite Topochemical Conversion Reaction. Based on the above results, the Aurivillius to perovskite topochemical conversion is proposed to occur in two sequential stages, shown in Figure 10.

In the first stage, the perovskite phase forms by multiple topotactic nucleation events, either directly on the precursor phase or on a related intermediate phase, which also forms by multiple nucleation on the precursor surface. Although the nucleation event is topotactic, the growing perovskite crystallites do not maintain epitaxy with the precursor phase, and become slightly misaligned from the Aurivillius parent structure. The lack of epitaxy

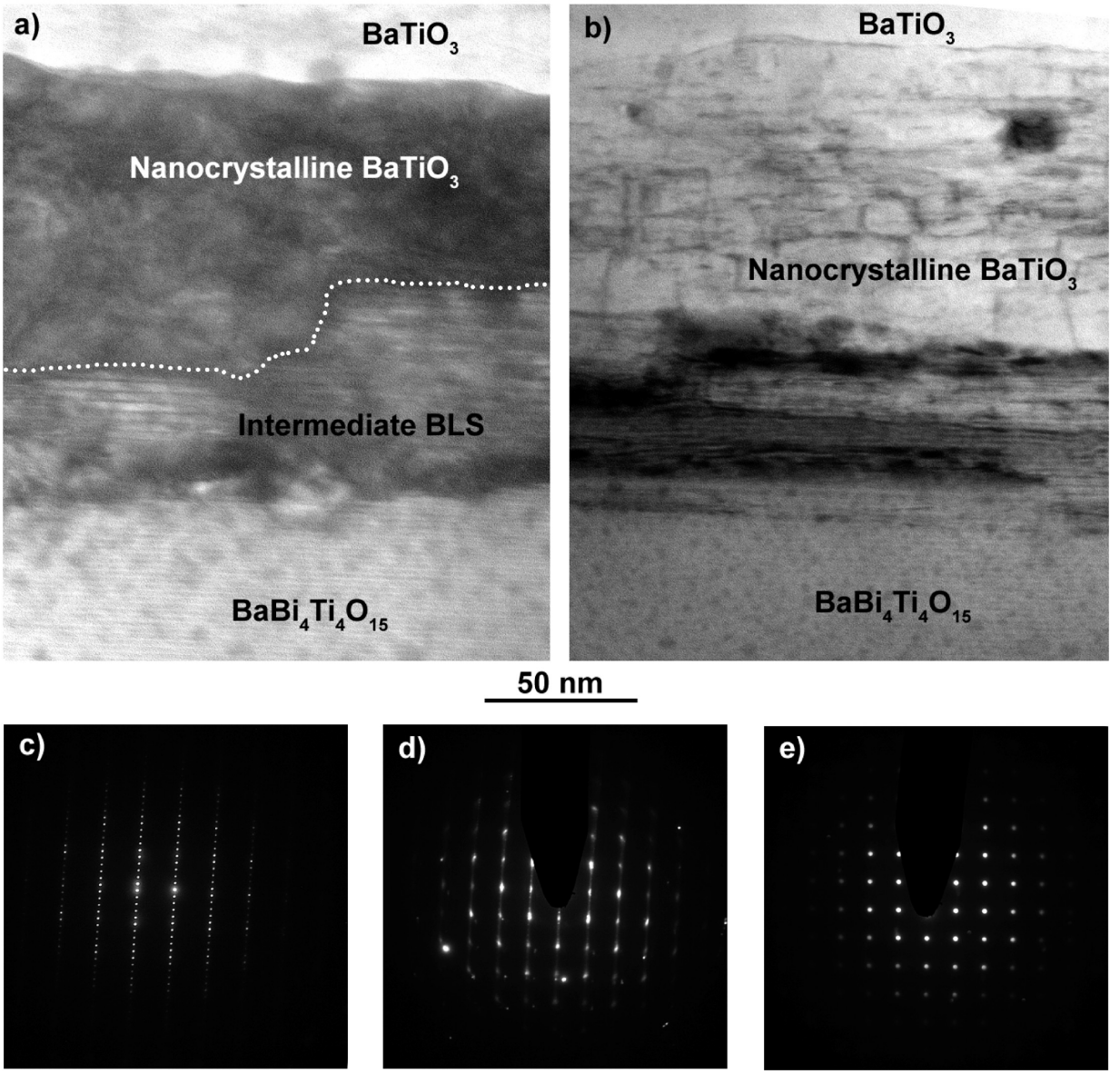

Figure 8. (a, b) Bright-field TEM showing detail at the $BaBi_4Ti_4O_{15}$ to $BaTiO_3$ reaction interface taken at slightly different instrument angles. (c−e) Electron diffraction patterns for $BaBi_4Ti_4O_{15}$, a region containing intermediate BLS phase(s), and $BaTiO_3$, respectively. The dotted line indicates the boundary between the intermediate BLS and $BaTiO_3$ phases.

is evidenced by boundary layers of >10 nm between the phases shown in Figures 8b and 9b. This boundary phase likely contains a Bi_2O_3-based liquid phase formed as a byproduct of the conversion reaction. Exfoliation of the partially converted microcrystals was observed in all systems, and can be seen by FESEM (Figure 6) as well as TEM (white voids in Figures 7 and 9). Because of the loss of epitaxy and exfoliation during topochemical conversion, the original microcrystal is replaced by an aligned perovskite-phase aggregate rather than a coherent single crystal. This stage of the TMC reaction is completed within a short time (<30 min) at the reaction temperature, as evidenced by the phase content of samples heated at 8 °C/min (Figure 4).

In the second stage of the TMC reaction, the aligned crystallites from the first stage recrystallize and sinter to form dense perovskite-phase platelets. The necessity of this process is evidenced by the long hold times used during successful TMC reactions (2−6 h), despite the complete formation of the perovskite phase within a much shorter time. In addition, samples heated for short times produced very fine, often high aspect ratio powders rather than coherent large platelets. The perovskite platelets resulting from topochemical conversion may be polycrystalline or single crystal in nature. The degree of grain misalignment (or mosaicity, in the case of near single crystal particles) is likely related to the initial misalignment of the perovskite crystallites after the first reaction stage as well as the temperature and time allowed for recrystallization and grain growth during the second stage. All perovskite microcrystals produced in this study ($NaNbO_3$, $PbTiO_3$, and $BaTiO_3$) show surface roughness well in excess of that shown by the Aurivillius precursor phases, that is not expected in single crystals. This roughness is taken as probable evidence of the polycrystalline or mosaic nature of these particles.

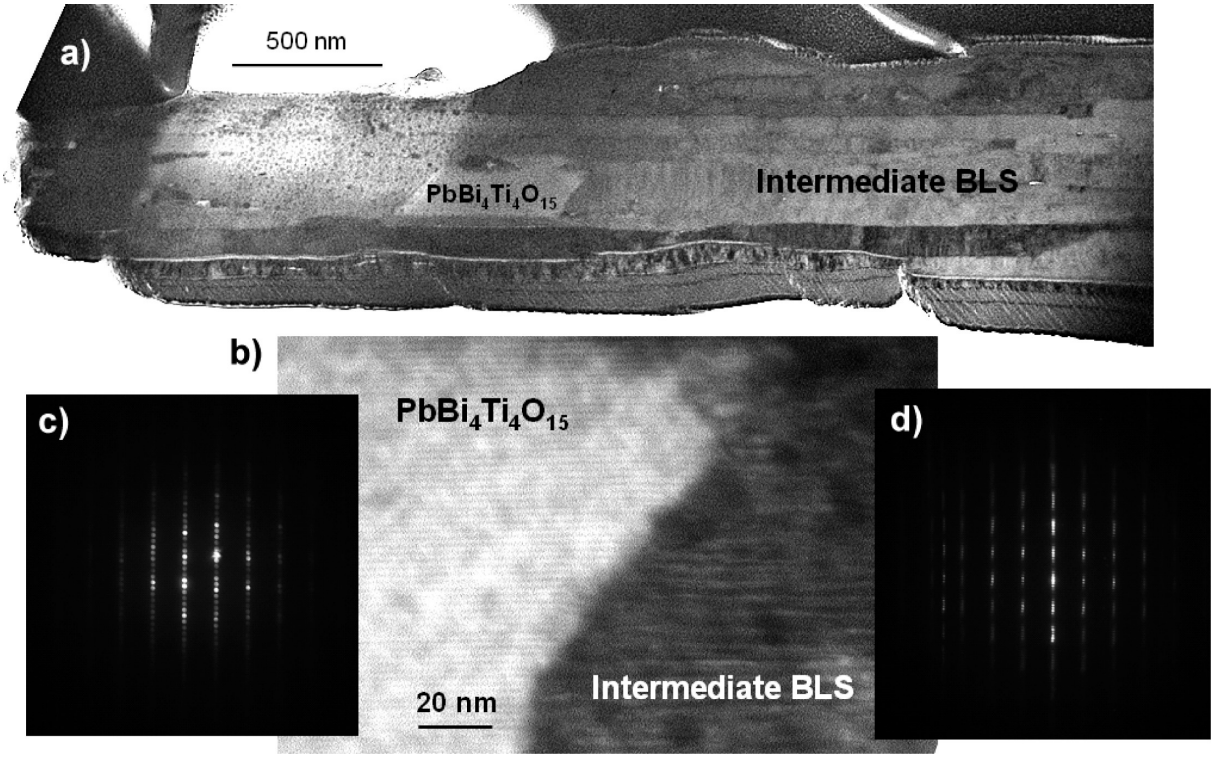

Figure 9. Bright-field TEM of a $PbBi_4Ti_4O_{15}$ particle mostly converted to an intermediate $PbTiO_3$−$PbBi_4Ti_4O_{15}$ phase, showing (a) the polycrystalline nature of the intermediate phase, (b) detail of the $PbBi_4Ti_4O_{15}$−intermediate phase boundary,and (c, d) diffraction patterns for $PbBi_4Ti_4O_{15}$ and the intermediate phase, respectively.

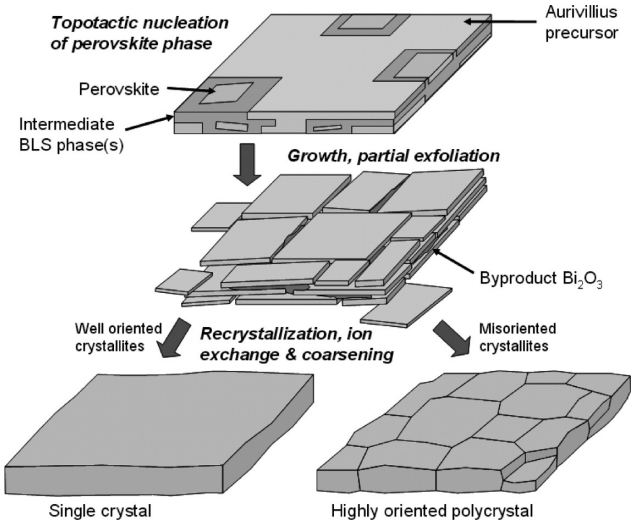

Figure 10. Schematic model of the Aurivillius to perovskite topochemical conversion reaction.

Conclusions

The reactions converting plate-like $BaBi_4Ti_4O_{15}$, $PbBi_4Ti_4O_{15}$, and $Na_{3.5}Bi_{2.5}Nb_5O_{18}$ Aurivillius microcrystals to the $BaTiO_3$, $PbTiO_3$, and $NaNbO_3$ perovskite phases were studied in detail. In general, the perovskite phase was observed to nucleate between 600 and 700 °C at multiple sites on each particle. During the formation of $BaTiO_3$ and $PbTiO_3$ perovskites, intermediate Aurivillius-type phases were observed to form. In particular, a persistent lead bismuth titanate compound with a $Bi_2O_2^{2+}$ layer spacing of around 78 Å prevented the formation of phase pure $PbTiO_3$ microcrystals. $BaTiO_3$ and $NaNbO_3$ microcrystals produced by topochemical conversion show high phase chemical and phase purity. Under TEM observation, reacted $BaBi_4Ti_4O_{15}$ and $PbBi_4Ti_4O_{15}$ particles both have some polycrystalline character, caused by imperfect alignment of growing nuclei of the perovskite or intermediate phases. In addition, FESEM micrographs show that Aurivillius phase particles exfoliate during topochemical conversion, most likely due to the expulsion of Bi_2O_3 and loss of epitaxy during this process. Long annealing times (1−6 h) at 950−1050 °C allow for recrystallization and grain growth of the aligned perovskite crystallites produced by topochemical conversion. The extent of misalignment and the time allowed for recrystallization determine whether the resulting particles are single crystal or polycrystalline in nature, as well as the final aspect ratio obtained. In all cases, the morphology of precursor Aurivillius phases can be maintained in the final microstructure.